Journal of Biomedical Optics

BiomedicalOptics.SPIEDigitalLibrary.org

Continuous-wave circular polarization terahertz imaging

Jillian P. Martin
Cecil S. Joseph
Robert H. Giles

SPIE.

Jillian P. Martin, Cecil S. Joseph, Robert H. Giles, "Continuous-wave circular polarization terahertz imaging," *J. Biomed. Opt.* **21**(7), 070502 (2016), doi: 10.1117/1.JBO.21.7.070502.

Continuous-wave circular polarization terahertz imaging

Jillian P. Martin,[a,b,*] Cecil S. Joseph,[a,b] and Robert H. Giles[a,b]
[a]University of Massachusetts Lowell, Department of Physics and Applied Physics, 136 Olney Science Center, 1 University Avenue, Lowell, Massachusetts 01854, United States
[b]Biomedical Terahertz Technology Center, 175 Cabot Street, Suite 114, Lowell, Massachusetts 01854, United States

Abstract. Biomedical applications of terahertz (THz) radiation are appealing because THz radiation is nonionizing and has the demonstrated ability to detect intrinsic contrasts between cancerous and normal tissue. A linear polarization-sensitive detection technique for tumor margin delineation has already been demonstrated; however, utilization of a circular polarization-sensitive detection technique has yet to be explored at THz frequencies. A reflective, continuous-wave THz imaging system capable of illuminating a target sample at 584 GHz with either linearly or circularly polarized radiation, and capable of collecting both cross- and copolarized signals remitted from the target, is implemented. To demonstrate the system's utility, a fresh *ex vivo* human skin tissue specimen containing nonmelanoma skin cancer was imaged. Both polarization-sensitive detection techniques showed contrast between tumor and normal skin tissue, although some differences in images were observed between the two techniques. Our results indicate that further investigation is required to explain the contrast mechanism, as well as to quantify the specificity and sensitivity of the circular polarization-sensitive detection technique. [DOI: 10.1117/1.JBO.21.7.070502]

Keywords: terahertz imaging; circular polarization; medical imaging; reflection imaging.

Paper 160306LR received May 16, 2016; accepted for publication Jun. 24, 2016; published online Jul. 14, 2016.

The terahertz (THz) regime lies between the infrared and microwave regions of the electromagnetic spectrum, spanning from 0.1 to 10 THz (3 mm to 30 μm). THz radiation is nonionizing and sensitive to water content; for these reasons, the idea of using THz radiation for imaging human tissue and delineating tumor margins has become an appealing topic in the biomedical field. A number of studies have examined the response of different types of human cancers to THz radiation and have shown the ability to differentiate between tumor and normal tissues.[1–9]

A reflective continuous-wave (CW) THz imaging system utilizing a linear polarization-sensitive detection technique has been demonstrated and used to delineate tumor margins for nonmelanoma skin cancer[2] and to determine reflectivity differences between normal and cancerous colons.[3] In this study, an optical system capable of illuminating *ex vivo* tissue specimens with either linearly polarized (LP) or circularly polarized (CP), CW THz radiation was designed and constructed to investigate the polarization-dependent interaction of THz radiation with human tissue. This system is a normal-incidence, raster-scanned imaging system, and was constructed using a 584-GHz laser source, a quarter-wave plate (QWP), a cryogenic bolometer, and an arrangement of polarizers. A tissue specimen was illuminated with LP and CP light at normal incidence, and amplitude intensity plots of the co- and crosspolarized reflected radiations were generated. This technique has been demonstrated at optical wavelengths,[10] where the scattering of light within the tissue volume has been extensively studied; however, it has yet to be implemented using THz radiation. Akin to the linear polarization-sensitive detection scheme demonstrated by Refs. 2 and 3, the optical system in this study collects both copolarized and crosspolarized signals remitted from tissue specimens mounted in a custom-designed sample holder. The optical interfaces of this sample holder are outlined in the boxed inset (dashed line) in Fig. 1. During imaging, this holder is mounted onto an XY scan stage and raster scanned across the focus of the THz beam at normal incidence. In this geometrical configuration, strong Fresnel reflections from the sample holder interfaces are generated. To remove reflections from these interfaces, a linear polarization-sensitive detection technique can be used, which only collects the crosspolarized signal remitted from a sample and discards the copolarized signal. However, by completely discarding the copolarized signal, the linear polarization-sensitive detection technique loses a large portion of the radiation weakly scattered from the tissue volume. A circular polarization-sensitive detection technique has the potential to separate specular reflections from weakly scattered radiation more effectively than the aforementioned technique because it is expected that radiation weakly scattered from superficial tissue layers will retain its original helicity, while the helicity of the radiation reflected from optical interfaces will be reversed.

In this study, tissue specimens were illuminated at 584 GHz using a CO_2 optically pumped far-infrared (FIR) molecular gas laser. The vertically polarized, 584 GHz, laser line chosen was generated by pumping formic acid (HCOOH) in the FIR laser cavity with the 9R28 transition of the CO_2 laser. The power measured at the FIR laser output was 10.23 mW. To generate a Gaussian beam profile, a dielectric tube was placed at the FIR laser output.[11] CP THz radiation was generated using a crystalline quartz QWP designed for CW THz radiation centered at 513 μm. This QWP was especially designed such that certain incident angles generate quarter-wave retardation without the need for antireflective coatings.[12] Signals remitted from tissue specimens were collected using a liquid helium-cooled silicon bolometer (IRLabs) with noise equivalent power of 1.13×10^{-13} W/Hz$^{1/2}$ and responsivity of 2.75×10^5 V/W.

The optical setup for this study employed two illumination channels: a CP illumination channel and an LP illumination channel. Each illumination channel utilized two detection channels: a copolarized channel and a crosspolarized channel. In regards to CP illumination, the copolarized remitted signal was defined as the CP component with the same helicity as the CP light incident on the target sample. In turn, the CP

*Address all correspondence to: Jillian P. Martin, E-mail: jillian_martin1@student.uml.edu

1083-3668/2016/$25.00

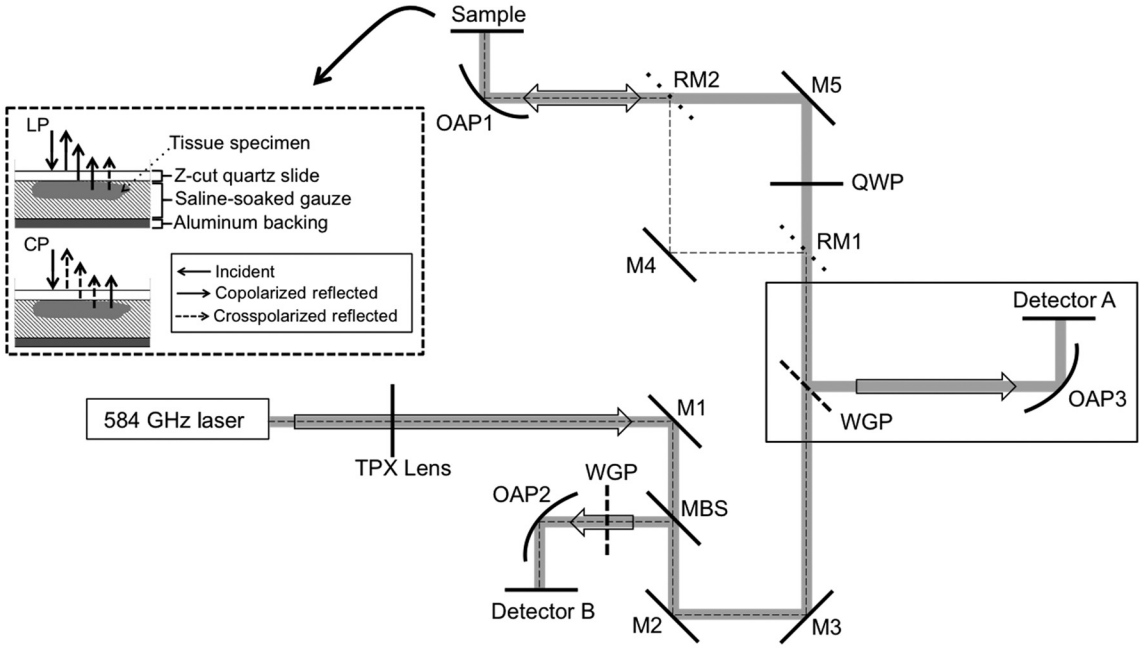

Fig. 1 Diagram of optical setup for THz polarization imaging. Optical components include: OAP mirrors, an MBS, a free-standing WGP, fixed mirrors (M), RM, and a quartz QWP. The boxed inset (dashed line) depicts a mounted tissue specimen and outlines the optical interfaces of the sample holder.

component with reversed helicity was defined as the crosspolarized signal. This same convention was used for defining the copolarized and crosspolarized signals remitted from target samples in response to LP illumination. A diagram of the optical setup is shown in Fig. 1 and is described as follows. The vertically polarized THz radiation exiting the FIR cavity was collimated using a 43-cm focal-length, polymethylpentene (TPX®) lens. This collimated beam was passed through a 50/50-mylar beam splitter (MBS) and focused onto the sample plane at normal incidence using a 7.6-cm focal-length, off-axis parabolic (OAP) mirror. Tissue specimens were mounted onto a computerized two-axis scan stage and raster scanned across the focus of the THz beam with a resolution of 0.15 mm and a dwell time of 100 ms per point. Software, written using NI LabVIEW™, was used to coordinate motion control and data acquisition to generate amplitude intensity plots of tissue specimens. To improve the system signal-to-noise ratio (SNR), a lock-in amplifier was used.

For LP illumination, the vertically polarized radiation was focused onto the sample plane at normal incidence via a system of removable mirrors (RM), indicated by the dashed line in Fig. 1. The signal remitted from the target sample was propagated back through the system of RM, until it reached the MBS. At the MBS, a portion of the remitted signal was reflected and passed through a free-standing, wire-grid polarizer (WGP) (Specac) with an aperture diameter of 16.5 mm, and wire width and periodicity of 10 and 25 μm, respectively. Depending on the orientation of the WGP, either copolarized or crosspolarized radiation was transmitted and collected by the bolometer, located at detector B in Fig. 1.

For CP illumination, the RM were taken out of the system and the vertically polarized radiation was propagated through a QWP, indicated by the thick gray line in Fig. 1. The QWP was oriented such that the vertically polarized radiation was transformed into CP radiation with an ellipticity (vertical-to-horizontal polarization ratio) of 1.04 for an incident angle of 4.7 deg with respect to the unit normal of the plate. The CP radiation was focused onto the sample plane at normal incidence. The signal remitted by the target sample was propagated back through the system, passing through the QWP, which transformed the right and left CP components into two orthogonal LP components. By placing a WGP oriented at 45 deg after the QWP, the crosspolarized signal was reflected and collected by the bolometer placed at detector A, shown boxed (solid line) in Fig. 1. To collect the copolarized signal, the WGP placed after the QWP was removed and both co- and crosspolarized signals propagated to the MBS, where they were reflected. Upon reflection, the signals passed through a WGP oriented such that only the copolarized signal was transmitted and collected by the bolometer placed at detector B.

For both LP and CP illumination, two amplitude intensity images were generated: a copolarized image and a crosspolarized image. Images were calibrated by measuring the full-scale return signal from a flat, front-surface mirror positioned in the sample plane for both illumination channels. The measured system SNR for the LP channels was 46 dB, while the SNRs corresponding to the copolarized and crosspolarized detection arms for CP illumination were 37 and 46 dB, respectively.

The size of the THz beam at the sample plane was measured by performing a knife-edge transmission scan on a thin metal plate placed in the focal plane. The knife-edge data yielded full width at half maximum values of 0.49 and 0.53 mm for the LP and CP illumination channels, respectively. Both illumination channels were focused to the same imaging plane. The beam waists corresponding to the LP and CP illumination channels were 0.42 and 0.45 mm, respectively.

To demonstrate the system's utility, a fresh human skin specimen containing nonmelanoma skin cancer was imaged. The specimen was obtained within 2 h following Mohs Micrographic surgery at Massachusetts General Hospital under an IRB approved protocol. Specimens were transferred to the University of Massachusetts Lowell within 45 min, where

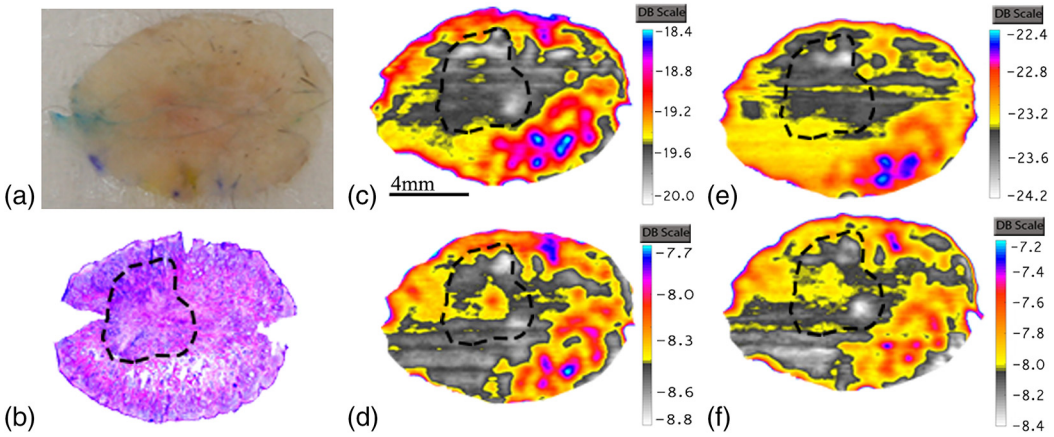

Fig. 2 (a) Photograph of skin specimen with z-cut quartz cover slide and saline-soaked gauze backing. (b) H&E-stained histology with dotted line demarcating tumor region. THz reflectance images corresponding to (c) crosspolarized and (d) copolarized detection arms for LP illumination and to (e) copolarized and (f) crosspolarized detection arms for CP illumination. Dotted lines in THz reflectance images demarcate tumor region, as diagnosed from the H&E histology.

skin samples were thawed and mounted. To prevent tissue dehydration during imaging, a custom-designed sample holder was used to sandwich skin tissue specimens between a 1-mm-thick, z-cut quartz slide and buffered saline-soaked gauze.[2,3] For histological processing, specimens were frozen and cut using an en face sectioning technique.[13] Frozen tissue sections, 5-μm thick, were placed on glass slides and stained with hematoxylin and eosin (H&E). These slides were then compared to the THz images obtained.

Figure 2 contains a photograph of a skin specimen containing basal cell carcinoma (BCC), along with the corresponding H&E-stained histology and the THz reflectance images obtained. During postprocessing, a bilinear interpolation, followed by a Gaussian low pass filter at one standard deviation, was applied to the THz images using MATLAB® software. The final images are displayed in logarithmic space, with off-sample areas removed. The dotted line in each of the images demarcates the tumor region, as diagnosed from the H&E-stained histology.

The skin specimen shown contains a rip in the upper right. This tear was pressed closed when the sample was mounted into the holder; nevertheless, it is likely some saline leaked through the rip during imaging, accounting for the low reflectivity regions observed in the upper right of the crosspolarized LP and copolarized CP images that lie outside the tumor outline. The crosspolarized LP and copolarized CP THz reflectance images do not contain strong signals from the optical interfaces of the sample holder (air-quartz and quartz-tissue/gauze interfaces), and thus predominantly contain signal from the tissue volume. However, the copolarized LP and crosspolarized CP THz reflectance images contain strong signals from the Fresnel reflections at optical interfaces. Consequently, signal levels measured in the detection channels containing Fresnel reflections are much higher than those measured in the channels which do not contain Fresnel reflections.

The correlation observed between the histology tumor diagnosis and regions of low reflectivity in the THz crosspolarized LP image in this study was in agreement with results obtained by Joseph et al.[2] In addition, correlation was observed between low reflectivity regions in the THz copolarized CP image and the THz crosspolarized LP image. Correlation between these THz images was expected prior to the start of this investigation on the basis that both copolarized CP and crosspolarized LP detection channels do not contain Fresnel reflections. While the mechanism behind the contrast observed between normal and cancerous tissue at THz frequencies is not yet well understood, several studies have been performed and have obtained results that indicate the contrast could be a result of a combination of differences in water content and differences in tissue structure. Wallace et al.[5] observed contrast between normal tissue and BCC using THz-pulsed imaging and reported that while the contrast was consistent with differences in water content, it may not be the only factor. Several groups have examined dehydrated and paraffin-embedded tissue at THz frequencies and have observed contrast between normal and cancerous tissue.[4,7–9] In particular, Bauer et al.[9] examined THz radiation diffracted and scattered from canine tissue using THz darkfield imaging and observed contrast between tumor and normal tissue, which had been formalin fixed, alcohol dehydrated, and embedded in paraffin wax. Moreover, Sy et al.[14] provided further evidence that contrast observed at THz frequencies is due to both differences in water content and differences in tissue structure in their investigation on the correlation between THz properties, water content, structural changes, and cirrhosis in liver tissue. This group observed contrast between healthy and cirrhotic liver tissues in both fresh and formalin-fixed specimens, and determined structural changes contributed up to 66% of the total change in the absorption coefficient at 0.4 THz.

Differences in structure between normal tissue and tumor is a potential explanation for the contrast observed in "non-Fresnel" detection channels; namely, the contrast that appears in crosspolarized LP and copolarized CP images obtained in studies utilizing polarization-sensitive detection techniques.[2,3] At THz frequencies, normal skin is heterogeneous due to the highly structured nature of the dermis, whereas tumor is characterized by a loss of structure and, thus, appears more homogeneous. Consequently, normal skin will scatter radiation more at THz frequencies due to higher local variation in refractive index, while tumors will exhibit less scattering due to comparatively lower refractive index variation.[2]

A final point for discussion arises upon comparing the measured signal levels in the crosspolarized LP image and the copolarized CP image. Remitted signal levels measured in the crosspolarized LP image varied between −18.4 and −20.0 dB, while signal levels corresponding to the copolarized CP image

varied between −22.4 and −24.2 dB. Prior to the start of this study, it was initially hypothesized that the CP-sensitive detection technique would separate specular reflections from weakly scattered radiation more effectively than the LP sensitive detection technique, accordingly leading to higher signal levels in the copolarized CP image. Instead, the results showed higher signal levels in the crosspolarized LP image as compared to the copolarized CP image. A possible explanation for this result is that, due to polarization memory effects,[15] the CP radiation penetrated the tissue to a greater depth than the LP radiation and remitted signals for CP illumination experienced greater attenuation than signals generated in response to LP illumination. This difference in penetration depth has been examined at optical wavelengths,[10] but has yet to be investigated at THz frequencies. This explanation may account for differences in signal levels as well as differences observed in the size and shape of bulk refractive index variations across a sample. Further research is required to confirm this explanation.

To summarize, a reflective CW THz imaging system capable of illuminating fresh *ex vivo* tissue samples with either LP or CP radiation was constructed. To the best of our knowledge, this is the first study to explore the interaction of CP THz radiation with fresh human skin tissue specimens. Correlation was observed between the sample histology and the THz crosspolarized LP reflectance image and was in agreement with the results obtained by Joseph et al.[2] Additionally, correlation was observed between the copolarized CP and crosspolarized LP THz reflectance images, thus demonstrating that a CP illumination and polarization-sensitive detection technique may be capable of differentiating between normal and cancerous tissue. Further investigation is required to explain the mechanism behind the contrast observed in this study and a larger number of tissue specimens need to be examined to determine the specificity and sensitivity of the circular polarization-sensitive detection technique implemented in this study.

Acknowledgments

The authors are grateful to Dr. Victor Neel for providing the skin specimen and outlining the tumor in the histology; to Julie O'Neill for preparing the histology slides; and to undergraduate student Will Chambers for assisting with image postprocessing. The authors would also like to thank Dr. Anna Yaroslavsky for her expertise in skin imaging, and her student, Nathan Perry, for mosaicing the histology images.

References

1. C. Yu et al., "The potential of terahertz imaging for cancer diagnosis: a review of investigations to date," *Quant. Imaging Med. Surg.* **2**(1), 33–45 (2012).
2. C. S. Joseph et al., "Imaging of ex vivo nonmelanoma skin cancers in the optical and terahertz spectral regions," *J. Biophotonics* **7**, 295–303 (2014).
3. P. Doradla et al., "Detection of colon cancer by continuous-wave terahertz polarization imaging technique," *J. Biomed. Opt.* **18**(9), 090504 (2013).
4. F. Wahaia et al., "Detection of colon cancer by terahertz techniques," *J. Mol. Struct.* **1006**, 77–82 (2011).
5. V. P. Wallace et al., "Terahertz pulsed spectroscopy of human basal cell carcinoma," *Appl. Spectrosc.* **60**, 1127–1133 (2006).
6. R. M. Woodward et al., "Terahertz pulse imaging of ex vivo basal cell carcinoma," *J. Invest. Dermatol.* **120**, 72–78 (2003).
7. Y. Ishikawa et al., "Terahertz spectroscopic imaging of liver cancer using ring cavity THz-wave parametric oscillator," in *Quantum Electronics Conf.*, 1236, IEEE (2005).
8. P. Knoblock et al., "Medical THz imaging: an investigation of histopathological samples," *Phys. Med. Biol.* **47**, 3875–3884 (2002).
9. T. Bauer et al., "Terahertz dark-field imaging of biomedical tissue," *Opt. Express* **9**, 616 (2001).
10. S. P. Morgan et al., "Surface-reflection elimination in polarization imaging of superficial tissue," *Opt. Lett.* **28**, 114 (2003).
11. A. A. Danylov et al., "Transformation of the multimode terahertz quantum cascade laser beam into a Gaussian, using a hollow dielectric waveguide," *Appl. Opt.* **46**, 5051 (2007).
12. R. H. Giles, "Design of a submillimeter ellipsometer and application to the measurement of complex indices of refraction of materials," Ph.D. Thesis, University of Lowell (1986).
13. K. G. Gross et al., *Mohs Surgery: Fundamentals and Techniques*, Mosby, St. Louis, Missouri(1999).
14. S. Sy et al., "Terahertz spectroscopy of liver cirrhosis: investigating the origin of contrast," *Phys. Med. Biol.* **55**(24), 7587–7596 (2010).
15. F. C. MacKintosh et al., "Polarization memory of multiply scattered light," *Phys. Rev. B* **40**, 9342–9345 (1989).